




Research Article

Trajectory Planning of an Intermittent Jumping Quadruped Robot with Variable Redundant and Underactuated Joints

Jun Zhong ^{1,2}, Minzhou Luo,^{1,2} Jizhuang Fan ³, and Jie Zhao ³

¹College of Mechanical & Electrical Engineering, Hohai University, Changzhou, 213022 Jiangsu Province, China

²Jiangsu Key Laboratory of Special Robot Technology, Hohai University, China

³State Key Laboratory of Robotics and System, Harbin Institute of Technology, Harbin 150001, China

Correspondence should be addressed to Jun Zhong; zhongjun@hhu.edu.cn

Received 21 March 2018; Revised 4 June 2018; Accepted 19 June 2018; Published 17 September 2018

Academic Editor: Andy Annamalai

Copyright © 2018 Jun Zhong et al. This is an open access article distributed under the Creative Commons Attribution License, which permits unrestricted use, distribution, and reproduction in any medium, provided the original work is properly cited.

The jumping robot has been a hot research field due to its prominent obstacle-climbing ability and excellent capacity in terrain adaptation and autonomous movement. However, huge impact between the robot and the ground when landing may cause structure damage, unbalanced movement, and even system crash. Therefore, trajectory planning of the jumping process has been a great challenge in robotic research, especially for the robot with varying underactuated and redundant joints. An intermittent jumping quadruped robot driven by pneumatic muscle actuators (PMAs) and owning variable redundant and underactuated joints designed in a previous study is taken as the study object. This paper divides the problem of trajectory planning into trajectory planning in the centroid space and joint space. Trajectory planning of different jumping phases in the centroid space adopts the scheme of minimizing the peak reaction force from the ground, then trajectory planning of the joint space is performed obeying the principle of minimizing consumed active torques. A jumping experiment is performed and validates the effectiveness of the proposed trajectory algorithm.

1. Introduction

Legged robots have been a hot research field due to excellent mobility on rugged terrain [1–3]. These robots have various motion modes, such as running, hopping, walking, and jogging [4–6]. In the case of stepping over barriers, hopping is an attractive choice. However, trajectory planning of leg robots faces some challenges, such as posture controlling in the airborne phase and huge collision impact with the ground when landing. Different planning methods have been proposed [7–10]. Wan et al. proposed an optimized jumping motion of a four-leg robot and analyzed numerical optimization results for different takeoff postures [11]. Xu et al. proposed a concept of inertial matching ellipsoid and directional manipulability to optimize the trajectory for a four-link planar mobile robot [12]. Heerden and Kawamura adopted the A-star path planning algorithm to realize jumping trajectory generation considering reducing backwards and compliant landing [13]. Kawamura and Heerden realized limiting referential torques to prevent tipping,

sliding, twisting, and excessively large ground collisions [14]. Aversa et al. introduced the generalized Jump-Point-Search algorithm to solve the problem of inventory-driven pathfinding [15]. Lakatos et al. dealt with the velocity control and planning of the bang-bang control parameters of the hopping robot [16]. Besides trajectory planning of jumping robots, many other scientists studied trajectory planning for the robotic manipulator and vehicle [17–22]. Constantinescu and Croft proposed an autonomous obstacle-avoidance function to plan trajectory and enhance the intelligence of a robotic manipulator [18]. In [19], a teleoperated robot system followed the trajectory planned by EMG signals of operators. Lolla et al. developed a time-optimal path planning method in dynamic flows using level set equations for multiple vehicles [23].

An intermittent jumping quadruped robot driven by pneumatic muscle actuators (PMAs) and owning variable redundant and underactuated joints (shown in Figure 1) has been proposed in our previous research. The robot weighs 4.658 kg with body length of 475 mm, body width of

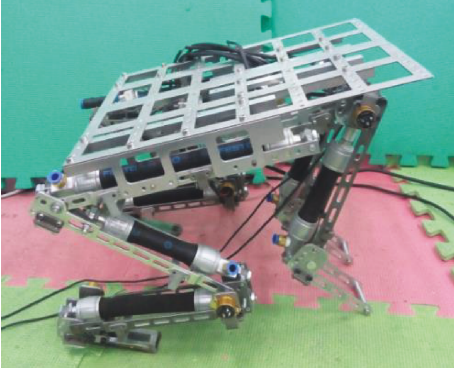


FIGURE 1: The intermittent jumping quadruped robot.

330 mm, foot length of 121 mm, shank length of 229 mm, thigh length of 249 mm, big arm of 248 mm, and small arm of 132 mm. The robot in the jumping process is a highly nonlinear dynamic system, and the complete jumping process can be divided to different continuous subphases and discrete subphases according to varying constraints and freedoms. Therefore, motion planning should be performed in different jumping subphases.

This paper deals with the trajectory planning in the centroid space firstly, then joint trajectory is planned in the joint space. The paper is organized in the following structures. Section 1 builds up the complete dynamic characteristics of the robot, Section 2 plans trajectory in the centroid space and joint space, and Section 3 performs the jumping experiment according to the given planned trajectory. Finally, the conclusion is drawn in Section 4.

2. Dynamic Modeling of the Intermittent Jumping Quadruped Robot

Each rear leg has three active joints whilst each foreleg has two active joints. The robot can be abstracted to be a planar six-bar mechanism with varying underactuated and redundant joints along with the jumping process (shown in Figure 2). When the robot lands, tiptoes will collide with the ground and a huge impact force acts on the robot, which stops the motion of the collision point in an immediately short time. This collision process can be described by impact dynamics theory. Discrete Lagrange dynamical principle is a widely used theory to depict the collision status. This research employs discrete Lagrange dynamic theory to build up a collision equation of the robot when it lands. In other motion stages, i.e., the takeoff phase, airborne phase, and landing phase, position, velocities, and acceleration change continuously. Dynamics of other motion stages are depicted by continuous dynamics. Besides, considering the contact status with the ground, the jumping process of the robot can be divided into the takeoff phase, airborne phase, and landing phase (shown in Figure 3). The landing phase consists of the collision I subphase, landing I subphase, collision II subphase, landing II subphase, collision III subphase, and landing III subphase. Hence, continuous phases adopt the continuous Lagrange dynamical principle, while dynamics

of landing impact phases (i.e., collision I subphase, collision II subphase, and collision III subphase) should be established using the discrete Lagrange dynamical principle.

The dynamic equation describing impact status between the robot and ground is described as follows:

$$D_e(q_s)\ddot{q}_s + C_e(q_s, \dot{q}_s)\dot{q}_s + G_e(q_s) + K_e(q_s) = \tau_e + \delta F_{\text{ext}}, \quad (1)$$

where $D_e(q_s)$ is the collision inertial matrix, $C_e(q_s)$ is the collision centrifugal matrix, $G_e(q_s)$ is the gravity matrix, $K_e(q_s)$ is the spring elastic force matrix, and $\tau_e(q_s)$ is the joint driving torque matrix.

Generalized joint velocities after collision can be drawn from

$$\dot{q}_s^+ = \dot{q}_s^- + D_e^-(q_s)J_e^T(q_s)[J_e(q_s)D^{-1}(q_s)J_e^T(q_s)]^{-1}\Delta\dot{X}_e(q_s). \quad (2)$$

Continuous dynamics is established as follows:

$$D(q_s)\ddot{q}_s + C(q_s, \dot{q}_s)\dot{q}_s + G(q_s) + K(q_s) = \tau, \quad (3)$$

where $D(q_s)$ is the positive definite matrices of inertia with dimension 8×8 ; $C(q_s, \dot{q}_s)$ is the first-order differential matrix, coefficient matrix of Coriolis force, and centrifugal force; $G(q_s)$ is the gravity matrix; $K(q_s)$ is the elastic force matrix of springs in the robot; τ is the generalized joint torque matrix $\tau = [\tau_1 \ \tau_2 \ \tau_3 \ \tau_4 \ \tau_5 \ \tau_6 \ f_{Ax} \ f_{Ay}]^T$; and f_{Ax} and f_{Ay} are the components on the horizontal and vertical directions, respectively, of the ground reaction.

From the analysis of a complete jumping process, the takeoff phase owns a single underactuated joint, both the airborne phase and collision I subphase have three underactuated joints, and the collision II subphase has a single underactuated joint while no underactuated joint exists in the collision III subphase. More details about the dynamic modeling and underactuated joints can be referred in [24].

3. Trajectory Planning of the Intermittent Jumping Quadruped Robot

Trajectory planning of different jumping phases in the task space adopts the scheme of minimizing the peak reaction force from the ground, then trajectory planning of the joint space would be performed obeying the principle of minimizing consumed active torques.

3.1. Trajectory Planning in the Task Space of the Robot. Trajectory of the mass center should be planned in the takeoff phase, airborne phase, landing I subphase, landing II subphase, and landing III subphase. Obviously, the mass center of the robot moves in projectile motion during the airborne phase and builds up a bridge connecting the takeoff phase and landing I subphase. Motion parameters of the robot at the start instant of the airborne phase equal to those at the end time of the takeoff phase, whilst motion parameters at the end time of the airborne phase are identical to those at the instant before impact to the ground. Hence,

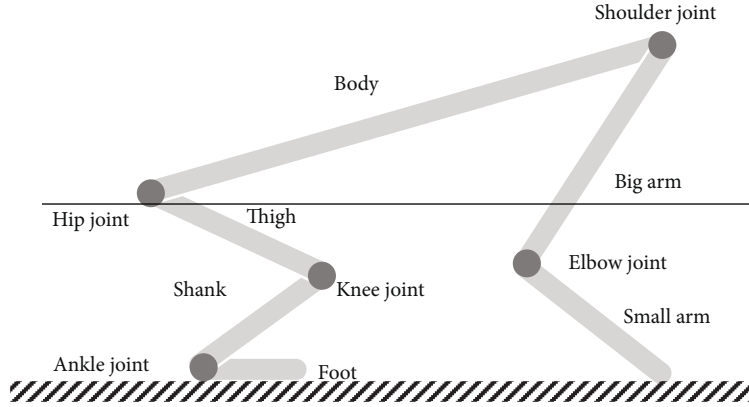


FIGURE 2: Equivalent six-bar-mechanism model of the robot.

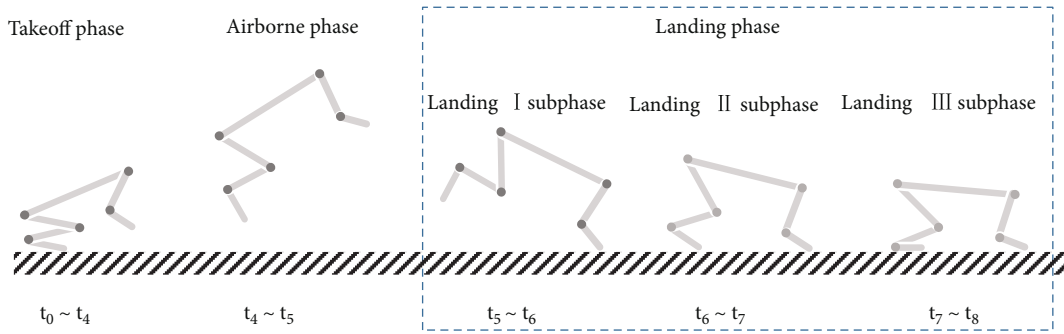


FIGURE 3: Jumping process of the robot.

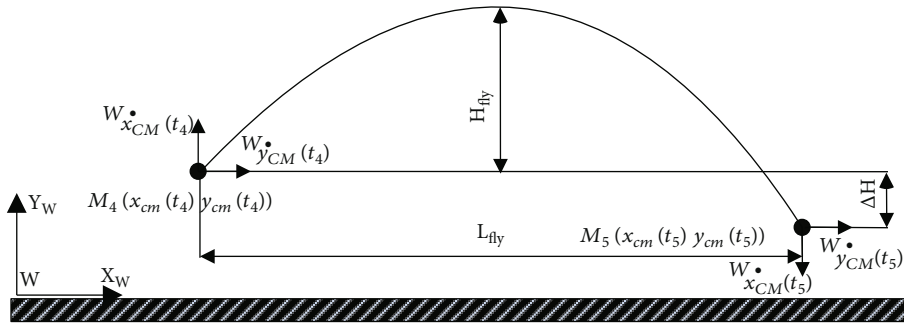


FIGURE 4: Mass-center trajectory of the airborne phase.

mass-center trajectory in the airborne phase would be planned firstly.

3.1.1. Trajectory Planning at the Airborne Phase. Ignoring air drag, the trajectory of the mass center of the robot is shown in Figure 4. Considering maximum jumping height H_{fly} of the mass center, centroid coordinate $M_4({}^W x_{CM}(t_4), {}^W y_{CM}(t_4))$, and centroid coordinate $M_5({}^W x_{CM}(t_5), {}^W y_{CM}(t_5))$ at the landing instant, initial velocity in the Y direction at the airborne phase is calculated as follows:

$${}^W \dot{y}_{CM}(t_4) = \sqrt{-2gH_{fly}}. \quad (4)$$

Time consumed at the airborne phase $t_{fly} = t_5 - t_4$ is calculated as follows:

$${}^W y_{CM}(t_5) = {}^W \dot{y}_{CM}(t_4) \cdot t_{fly} + 0.5gt_{fly}^2. \quad (5)$$

Velocity in the horizontal direction at the airborne phase is as follows:

$${}^W \dot{x}_{CM} = \frac{{}^W x_{CM}(t_5) - {}^W x_{CM}(t_4)}{t_{fly}}. \quad (6)$$

Velocity at the end instant of the airborne phase (i.e., M_5) is acquired according to oblique projectile motion as follows:

$$\begin{cases} {}^W\dot{x}_{CM}(t_5) = {}^W\dot{x}_{CM}(t_4), \\ {}^W\dot{y}_{CM}(t_5) = {}^W\dot{y}_{CM}(t_4) + gt_{\text{fly}}. \end{cases} \quad (7)$$

3.1.2. Trajectory Planning at the Takeoff Phase. Motion trail of the center mass of the robot at the takeoff phase is continuous. Given the centroid coordinate and velocity at the end instant of the takeoff stage (i.e., t_4) and time $t_{\text{jump}} = t_4 - t_1$ consumed in the takeoff stage, the centroid trajectory can be planned by minimizing the peak reaction force from the ground with the purpose of reducing damage to the robot mechanism. This paper adopts an eight-polynomial form to describe the mass-center trajectory:

$$\begin{aligned} {}^W\dot{X}_{CM} &= \begin{bmatrix} {}^W\dot{x}_{CM} \\ {}^W\dot{y}_{CM} \end{bmatrix} \\ &= \begin{bmatrix} a_8t^8 + a_7t^7 + a_6t^6 + a_5t^5 + a_4t^4 + a_3t^3 + a_2t^2 + a_1t + a_0 \\ b_8t^8 + b_7t^7 + b_6t^6 + b_5t^5 + b_4t^4 + b_3t^3 + b_2t^2 + b_1t + b_0 \end{bmatrix}, \\ &t \in [t_1, t_4]. \end{aligned} \quad (8)$$

a_i and b_i are parameters to be optimized. The objective function is as follows:

$$\begin{aligned} J &= \min \left\{ \kappa_1 \max \left(\vec{f}_{Gx} \right) + \kappa_2 \max \left(\vec{f}_{Gy} \right) \right\} \\ &= \min \left\{ \kappa_1 \max \left(M {}^W\ddot{x}_{CM} \right) + \kappa_2 \max \left[M \left({}^W\ddot{y}_{CM} + g \right) \right] \right\}. \end{aligned} \quad (9)$$

f_{Gx} and f_{Gy} are the horizontal component force and vertical component force, respectively, of the ground reaction on the centroid. Weight parameters κ_i ($i = 1, 2$) satisfy the condition

$$\kappa_1 + \kappa_2 = 1, \quad \kappa_i \in (0, 1). \quad (10)$$

The constraints consist of the initial position, velocity, and acceleration of the robot centroid. Furthermore, horizontal reaction of the ground should be equal to or less than the sliding friction force so as to avoid slipping at the takeoff stage, i.e., the constraints are as follows:

$$\begin{aligned} {}^W X_{CM}(t_1) &= {}^W X_{t_1}, \\ {}^W X_{CM}(t_4) &= {}^W X_{t_4}, \\ {}^W \dot{X}_{CM}(t_4) &= {}^W \dot{X}_{t_4}, \end{aligned}$$

$${}^W \dot{X}_{CM}(t_1) = 0,$$

$${}^W \ddot{X}_{CM}(t_1) = 0,$$

$${}^W \ddot{X}_{CM}(t_4) = [0 \ g]^T,$$

$$\ddot{y}_{CM} \geq g,$$

$$\left| \frac{{}^W \ddot{x}_{CM}}{{}^W \ddot{y}_{CM}} \right| \leq \mu,$$

(11)

where ${}^W X_{t_1}$ is the centroid displacement at the t_1 instant during the takeoff stage, ${}^W X_{t_4}$ is the centroid displacement at the t_4 instant during the takeoff stage, ${}^W \dot{X}_{t_4}$ is the centroid velocity at the t_4 instant during the takeoff stage, and μ is the ground sliding friction coefficient.

3.1.3. Trajectory Planning at the Landing Phase. Three collisions occur at the landing phase and produce sudden changes of joint velocities and centroid velocity. Hence, the landing stage can be divided into three subphases, i.e., landing I subphase, landing II subphase, and landing III subphase. Centroid trajectory of the robot should be optimized at these three subphases.

(1) Trajectory Planning at the Landing I Subphase. The centroid position at start instant t_5^+ of the landing I subphase equals that at the end moment t_5^- of the airborne phase. The centroid velocity at the t_5^+ instant after colliding is required from joint velocities after colliding, which could be calculated by colliding dynamics (2); the centroid acceleration at the t_5^+ instant after colliding is calculated from joint acceleration after colliding. The given time $t_{\text{landI}} = t_5^+ - t_6^-$ consumed at the landing I subphase, centroid position, velocity and acceleration at t_6^- , and parameters of an eight-polynomial form describing the mass-center trajectory could be optimized by minimizing the peak ground reaction:

$$\begin{aligned} {}^W\dot{X}_{CM} &= \begin{bmatrix} {}^W\dot{x}_{CM} \\ {}^W\dot{y}_{CM} \end{bmatrix} \\ &= \begin{bmatrix} a_8t^8 + a_7t^7 + a_6t^6 + a_5t^5 + a_4t^4 + a_3t^3 + a_2t^2 + a_1t + a_0 \\ b_8t^8 + b_7t^7 + b_6t^6 + b_5t^5 + b_4t^4 + b_3t^3 + b_2t^2 + b_1t + b_0 \end{bmatrix}, \\ &t \in [t_5^+, t_6^-]. \end{aligned} \quad (12)$$

a_i and b_i are parameters to be optimized. The objective function is as follows:

$$J = \min \left\{ \kappa_1 \max \left(\vec{f}_{Gx} \right) + \kappa_2 \max \left(\vec{f}_{Gy} \right) \right\} \quad (13)$$

Weight parameters κ_i ($i = 1, 2$) satisfy the condition

$$\kappa_1 + \kappa_2 = 1, \quad \kappa_i \in (0, 1). \quad (14)$$

The constraints are as follows:

$$\begin{aligned} {}^W X_{CM}(t_5^+) &= {}^W X_{t_5^+}, \\ {}^W X_{CM}(t_6^-) &= {}^W X_{t_6^-}, \\ {}^W \dot{X}_{CM}(t_5^+) &= {}^W \dot{X}_{t_5^+}, \\ {}^W \dot{X}_{CM}(t_6^-) &= {}^W \dot{X}_{t_6^-}, \\ {}^W \ddot{X}_{CM}(t_5^+) &= {}^W \ddot{X}_{t_5^+}, \\ {}^W \ddot{X}_{CM}(t_6^-) &= {}^W \ddot{X}_{t_6^-}, \\ \frac{{}^W \ddot{X}_{CM}}{{}^W \ddot{y}_{CM}} &\leq \mu. \end{aligned} \quad (15)$$

(2) *Trajectory Planning at the Landing II Subphase.* The centroid position at the start instant t_6^+ of the landing II subphase equals to that at the moment t_6^- when collision between the sole and the ground occurs. The centroid velocity at the t_6^+ instant after colliding is acquired from joint velocity after colliding, which could be calculated by colliding dynamics (2); the centroid acceleration at the t_6^+ instant after colliding is calculated from joint acceleration after colliding. An algorithm similar with that in Trajectory Planning at Landing I Subphase is adopted to plan trajectories at the landing II subphase:

$$\begin{aligned} {}^W \dot{X}_{CM} &= \begin{bmatrix} {}^W \dot{x}_{CM} \\ {}^W \dot{y}_{CM} \end{bmatrix} \\ &= \begin{bmatrix} a_8 t^8 + a_7 t^7 + a_6 t^6 + a_5 t^5 + a_4 t^4 + a_3 t^3 + a_2 t^2 + a_1 t + a_0 \\ b_8 t^8 + b_7 t^7 + b_6 t^6 + b_5 t^5 + b_4 t^4 + b_3 t^3 + b_2 t^2 + b_1 t + b_0 \end{bmatrix}, \\ &t \in [t_6^+, t_7^-]. \end{aligned} \quad (16)$$

a_i and b_i are parameters to be optimized. The objective function is as follows:

$$J = \min \left\{ \kappa_1 \max \left(\vec{f}_{Gx} \right) + \kappa_2 \max \left(\vec{f}_{Gy} \right) \right\}. \quad (17)$$

Weight parameters κ_i ($i = 1, 2$) satisfy the condition

$$\kappa_1 + \kappa_2 = 1, \quad \kappa_i \in (0, 1). \quad (18)$$

The constraints are listed as follows:

$$\begin{aligned} {}^W X_{CM}(t_6^+) &= {}^W X_{t_6^+}, \\ {}^W X_{CM}(t_7^-) &= {}^W X_{t_7^-}, \\ {}^W \dot{X}_{CM}(t_6^+) &= {}^W \dot{X}_{t_6^+}, \\ {}^W \dot{X}_{CM}(t_7^-) &= {}^W \dot{X}_{t_7^-}, \\ {}^W \ddot{X}_{CM}(t_6^+) &= {}^W \ddot{X}_{t_6^+}, \\ {}^W \ddot{X}_{CM}(t_7^-) &= {}^W \ddot{X}_{t_7^-}, \\ \frac{{}^W \ddot{X}_{CM}}{{}^W \ddot{y}_{CM}} &\leq \mu. \end{aligned} \quad (19)$$

(3) *Trajectory Planning at the Landing III Subphase.* Joint velocity after collision with the ground can be calculated using (2). Obviously, the centroid velocity and centroid acceleration at the t_7^+ instant can be calculated. The purpose of trajectory planning in the task space is to adjust the centroid to the desired position and make preparation for the next jumping movement. Given $t_{\text{land III}} = t_8 - t_7$ and the centroid position at the t_8 instant, parameters of the eight-polynomial form describing the mass-center trajectory could be optimized by minimizing the peak ground reaction:

$$\begin{aligned} {}^W \dot{X}_{CM} &= \begin{bmatrix} {}^W \dot{x}_{CM} \\ {}^W \dot{y}_{CM} \end{bmatrix} \\ &= \begin{bmatrix} a_8 t^8 + a_7 t^7 + a_6 t^6 + a_5 t^5 + a_4 t^4 + a_3 t^3 + a_2 t^2 + a_1 t + a_0 \\ b_8 t^8 + b_7 t^7 + b_6 t^6 + b_5 t^5 + b_4 t^4 + b_3 t^3 + b_2 t^2 + b_1 t + b_0 \end{bmatrix}, \\ &t \in [t_7, t_8]. \end{aligned} \quad (20)$$

a_i and b_i are parameters to be optimized. The objective function is as follows:

$$J = \min \left\{ \kappa_1 \max \left(\vec{f}_{Gx} \right) + \kappa_2 \max \left(\vec{f}_{Gy} \right) \right\}. \quad (21)$$

Weight parameters κ_i ($i = 1, 2$) satisfy the condition

$$\kappa_1 + \kappa_2 = 1, \quad \kappa_i \in (0, 1). \quad (22)$$

The constraints are as follows:

$$\begin{aligned} {}^W X_{CM}(t_7) &= {}^W X_{t_7}, \\ {}^W X_{CM}(t_8) &= {}^W X_{t_8}, \end{aligned}$$

$$\begin{aligned}
{}^W\dot{X}_{CM}(t_7) &= {}^W\dot{X}_{t_7}, \\
{}^W\dot{X}_{CM}(t_8) &= 0, \\
{}^W\ddot{X}_{CM}(t_7) &= {}^W\ddot{X}_{t_7}, \\
{}^W\ddot{X}_{CM}(t_8) &= 0, \\
\frac{{}^W\ddot{x}_{CM}}{{}^W\ddot{y}_{CM}} &\leq \mu.
\end{aligned} \tag{23}$$

3.2. Trajectory Planning in the Joint Space. Joint trajectory is required by mapping the planned trajectory in the task space. Because the jumping robot is a highly nonlinear complex system with redundant joints and underactuated joints, joint trajectory will be optimized by combination of robot dynamics and redundant properties. Besides, jumping posture at the initial state should be optimized according to the specified task.

3.2.1. Optimization of Initial Jumping Posture. The paper adopts the transmission property of motion of the mechanism at a given position in the operation space to measure the capacity of movement at a given direction. By using this principle, joint trajectory will be optimized to maximize the centroid velocity at a given direction while minimizing joint velocity. Using Jacobian matrix describing the relationship of the centroid velocity and joint velocity space, the unit ball is established as follows:

$$\dot{q}_s^T \dot{q}_s = 1. \tag{24}$$

Equation (24) can be rewritten by mapping to the task space:

$${}^W\dot{X}_{CM}^T \left(J_s^T J_s \right)^{-1} {}^W\dot{X}_{CM} = 1. \tag{25}$$

Equation (25) is the *operable ellipsoid of generalized velocity*. Assume the direction vector of the centroid velocity is $\vec{p} = [\cos \gamma_1 \ \cos \gamma_2]^T$, γ_1 and γ_2 representing angles between \vec{p} and two axes [X, Y] of a ground coordinate system, respectively. Obviously, the centroid velocity is rewritten as follows:

$${}^W\dot{X}_{CM} = A \cdot \vec{p}, \tag{26}$$

where A represents magnitude of the centroid velocity. Combining (25) and (26),

$$A \cdot \vec{p} \left(J_s^T J_s \right)^{-1} A \cdot \vec{p} = 1. \tag{27}$$

Define

$$DM = A^2 = \left[\vec{p} \left(J_s^T J_s \right)^{-1} \vec{p} \right]^{-1} \tag{28}$$

as the *manipulability of the centroid at direction \vec{p}* . The bigger the value of DM, the better the transmission capacity in the specified direction from the joint velocity space to the centroid velocity space. Given the contact constraint between the foreleg of the robot and the ground (i.e., the G point), the centroid trajectory, and change interval $[\Delta_{1i} \ \Delta_{2i}]$ ($i=1\sim 6$) of joint angles, the optimized function of the joint space is established as follows:

$$DM(q_1, \dots, q_6) = \max \left\{ \left[\vec{p} \left(J_s^T J_s \right)^{-1} \vec{p} \right]^{-1} \right\}. \tag{29}$$

The constraints are as follows:

$$\begin{aligned}
{}^W X_G(t_1) &= L_s, \\
{}^W Y_G(t_1) &= 0, \\
{}^W x_{CM}(t_1) &= \frac{\sum_{i=1}^6 m_i^A x_{cmi}}{\sum_{i=1}^6 m_i}, \\
{}^W y_{CM}(t_1) &= \frac{\sum_{i=1}^6 m_i^A y_{cmi}}{\sum_{i=1}^6 m_i}, \\
\Delta_{1i} &\leq \Delta q_i \leq \Delta_{2i}, \\
\tau_{idown} &\leq \tau_i \leq \tau_{iup}.
\end{aligned} \tag{30}$$

Given the time consumed in posture adjustment, initial joint velocities, and desired joint velocities, joint trajectories in a five-order polynomial form can be acquired from (30).

3.2.2. Trajectory Planning at the Takeoff Subphase. The trajectory in the joint space will be optimized according to the planned centroid trajectory and initial takeoff posture. ZMP principle is adopted to guarantee the takeoff stability [25, 26]. The eight-polynomial form is adopted to optimize the joint trajectory by minimizing total consumed active torque:

$$\begin{aligned}
q_i(t) &= a_{18}t^8 + a_{17}t^7 + a_{16}t^6 + a_{15}t^5 + a_{14}t^4 + a_{13}t^3 + a_{12}t^2 + a_{11}t + a_{10}, \\
t &\in [t_1, t_4].
\end{aligned} \tag{31}$$

a_i and b_i are parameters to be optimized. The objective function is as follows:

$$J = \min \left\{ \int_{t_1}^{t_4} \left(\sum_{i=2}^6 |\tau_i| \right) dt \right\}, \tag{32}$$

where $\tau_2 \sim \tau_6$ represent active torques of the knee joint, hip joint, shoulder joint, and elbow joint, respectively; t_1 and t_4 are the starting instant and end instant, respectively, of the takeoff phase.

The constraints are as follows:

$$\begin{aligned}
& {}^W x_A = {}^W y_A = 0, \\
& q_i(t)|_{t=t_1} = q_i(t_1), \\
& \dot{q}_i(t)|_{t=t_1} = 0, \\
& \ddot{q}_i(t)|_{t=t_1} = 0, \\
& {}^W x_{\text{CM}}(t) = \frac{\sum_{i=1}^6 m_i {}^W x_{\text{cmi}}(t)}{\sum_{i=1}^6 m_i}, \\
& {}^W y_{\text{CM}}(t) = \frac{\sum_{i=1}^6 m_i {}^W y_{\text{cmi}}(t)}{\sum_{i=1}^6 m_i}, \\
& {}^W \dot{x}_{\text{CM}}(t) = \frac{\sum_{i=1}^6 m_i {}^W \dot{x}_{\text{cmi}}(t)}{\sum_{i=1}^6 m_i}, \\
& {}^W \dot{y}_{\text{CM}}(t) = \frac{\sum_{i=1}^6 m_i {}^W \dot{y}_{\text{cmi}}(t)}{\sum_{i=1}^6 m_i}, \\
& {}^W \ddot{x}_{\text{CM}}(t) = \frac{\sum_{i=1}^6 m_i {}^W \ddot{x}_{\text{cmi}}(t)}{\sum_{i=1}^6 m_i}, \\
& {}^W \ddot{y}_{\text{CM}}(t) = \frac{\sum_{i=1}^6 m_i {}^W \ddot{y}_{\text{cmi}}(t)}{\sum_{i=1}^6 m_i}, \\
& X_{\text{ZMP}} \in S_{\text{contact}}, \\
& q_{\text{idown}} \leq q_i \leq q_{\text{iup}}, \\
& \tau_{\text{idown}} \leq \tau_i \leq \tau_{\text{iup}}.
\end{aligned} \tag{33}$$

3.2.3. Trajectory Planning at the Airborne Phase. The motion of drawing back the rear legs is done at the airborne phase to make preparation for landing. To mitigate collision between the foreleg and the ground, the kinematic energy of the tiptoe should be reduced. Considering limitations of driver power and structure design, it is difficult to reduce velocity of the tiptoe to zero; thus, this paper introduces two small parameters w_{Gx} and w_{Gy} to measure the reduction extent of the tiptoe velocity. The trajectories of active joints are depicted as follows:

$$\begin{aligned}
q_i(t) = a_{18}t^8 + a_{17}t^7 + a_{16}t^6 + a_{15}t^5 + a_{14}t^4 + a_{13}t^3 + a_{12}t^2 + a_{11}t + a_{10}, \\
t \in [t_4, t_5^-].
\end{aligned} \tag{34}$$

a_i and b_i are parameters to be optimized. The objective function is as follows:

$$J = \min \left\{ \int_{t_4}^{t_5^-} \left(\sum_{i=2}^6 |\tau_i| \right) dt \right\}. \tag{35}$$

The constraints are as follows:

$$\begin{aligned}
& q_i(t)|_{t=t_4} = q_i(t_4), \\
& \dot{q}_i(t)|_{t=t_4} = \dot{q}_i(t_4), \\
& \ddot{q}_i(t)|_{t=t_4} = \ddot{q}_i(t_4), \\
& {}^W \dot{x}_G(t_5^-) = w_{Gx} {}^W \dot{x}_G(t_4), \\
& {}^W \dot{y}_G(t_5^-) = w_{Gy} {}^W \dot{y}_G(t_4), \\
& {}^W x_{\text{CM}}(t) = \frac{\sum_{i=1}^6 m_i {}^W x_{\text{cmi}}(t)}{\sum_{i=1}^6 m_i}, \\
& {}^W y_{\text{CM}}(t) = \frac{\sum_{i=1}^6 m_i {}^W y_{\text{cmi}}(t)}{\sum_{i=1}^6 m_i}, \\
& {}^W \dot{x}_{\text{CM}}(t) = \frac{\sum_{i=1}^6 m_i {}^W \dot{x}_{\text{cmi}}(t)}{\sum_{i=1}^6 m_i}, \\
& {}^W \dot{y}_{\text{CM}}(t) = \frac{\sum_{i=1}^6 m_i {}^W \dot{y}_{\text{cmi}}(t)}{\sum_{i=1}^6 m_i}, \\
& {}^W \ddot{x}_{\text{CM}}(t) = \frac{\sum_{i=1}^6 m_i {}^W \ddot{x}_{\text{cmi}}(t)}{\sum_{i=1}^6 m_i}, \\
& {}^W \ddot{y}_{\text{CM}}(t) = \frac{\sum_{i=1}^6 m_i {}^W \ddot{y}_{\text{cmi}}(t)}{\sum_{i=1}^6 m_i}, \\
& \max |\alpha_4| - \min |\alpha_4| < 180^\circ, \\
& \alpha_4(t_5^-) \in [\alpha_4^{\text{down}}, \alpha_4^{\text{up}}], \\
& q_{\text{idown}} \leq q_i \leq q_{\text{iup}}, \\
& \tau_{\text{idown}} \leq \tau_i \leq \tau_{\text{iup}}.
\end{aligned} \tag{36}$$

3.2.4. Trajectory Planning at the Landing Stage. The landing stage is divided into the landing I subphase, landing II subphase, and landing III subphase according to three collisions between the robot and the ground. Hence, trajectory planning in the joint space will be performed at those three subphases.

(1) Joint Trajectory Planning at the Landing I Subphase. Joint angular displacements at the start instant t_5^+ of the landing I subphase equal those at the end instant t_5^- of the airborne phase. The joint velocity at the instant t_5^+ after collision can be calculated using (2), whilst joint angular accelerations can be required by (3). To minimize the collision between the tiptoe of the foreleg and the ground, two small parameters w_{Ax} and w_{Ay} are introduced to measure the reduction extent of the tiptoe velocity. The ZMP principle is adopted to guarantee the stability of the landing I movement. The trajectories of active joints are depicted as follows:

$$\begin{aligned}
q_i(t) = a_{18}t^8 + a_{17}t^7 + a_{16}t^6 + a_{15}t^5 + a_{14}t^4 + a_{13}t^3 + a_{12}t^2 + a_{11}t + a_{10}, \\
t \in [t_5^+, t_6^-].
\end{aligned} \tag{37}$$

a_i and b_i are parameters to be optimized. The object function is established to minimize the total consumed active torque as follows:

$$J = \min \left\{ \int_{t_5^+}^{t_6^-} \left(\sum_{i=2}^6 |\tau_i| \right) dt \right\}. \quad (38)$$

The constraints are listed as follows:

$$\begin{aligned} q_i(t)|_{t=t_5^+} &= q_i(t_5^+), \\ \dot{q}_i(t)|_{t=t_5^+} &= \dot{q}_i(t_5^+), \\ \ddot{q}_i(t)|_{t=t_5^+} &= \ddot{q}_i(t_5^+), \\ {}^W \dot{x}_A(t_6^-) &= w_{Ax} {}^W \dot{x}_A(t_5^+), \\ {}^W \dot{y}_A(t_6^-) &= w_{Ay} {}^W \dot{y}_A(t_5^+), \\ {}^W x_G &= L, \\ {}^W y_G &= 0, \\ {}^W \dot{x}_G &= {}^W \dot{y}_G = {}^W \ddot{x}_G = {}^W \ddot{y}_G = 0, \\ {}^W x_{CM}(t) &= \frac{\sum_{i=1}^6 m_i {}^W x_{cmi}(t)}{\sum_{i=1}^6 m_i}, \\ {}^W y_{CM}(t) &= \frac{\sum_{i=1}^6 m_i {}^W y_{cmi}(t)}{\sum_{i=1}^6 m_i}, \\ {}^W \dot{x}_{CM}(t) &= \frac{\sum_{i=1}^6 m_i {}^W \dot{x}_{cmi}(t)}{\sum_{i=1}^6 m_i}, \\ {}^W \dot{y}_{CM}(t) &= \frac{\sum_{i=1}^6 m_i {}^W \dot{y}_{cmi}(t)}{\sum_{i=1}^6 m_i}, \\ {}^W \ddot{x}_{CM}(t) &= \frac{\sum_{i=1}^6 m_i {}^W \ddot{x}_{cmi}(t)}{\sum_{i=1}^6 m_i}, \\ {}^W \ddot{y}_{CM}(t) &= \frac{\sum_{i=1}^6 m_i {}^W \ddot{y}_{cmi}(t)}{\sum_{i=1}^6 m_i}, \\ X_{ZMP} &\in S_{\text{contact}}, \\ q_{\text{down}} &\leq q_i \leq q_{\text{iup}}, \\ \tau_{\text{down}} &\leq \tau_i \leq \tau_{\text{iup}}. \end{aligned} \quad (39)$$

(2) *Joint Trajectory Planning at the Landing II Subphase.* Joint angular displacements at the start instant t_6^+ of the landing II subphase equal those at the end instant t_6^- of the landing I subphase. The joint velocity at instant t_6^+ after collision can be calculated using (2), whilst joint angular accelerations can be required by (3). To minimize the collision between the heel and the ground, two small parameters w_{Bx} and w_{By} are introduced to measure the

reduction extent of the heel velocity; trajectories of active joints are depicted as follows:

$$q_i(t) = a_{i8}t^8 + a_{i7}t^7 + a_{i6}t^6 + a_{i5}t^5 + a_{i4}t^4 + a_{i3}t^3 + a_{i2}t^2 + a_{i1}t + a_{i0}, \quad t \in [t_6^+, t_7^-]. \quad (40)$$

a_i and b_i are parameters to be optimized. The object function is established to minimize the total consumed active torque as follows:

$$J = \min \left\{ \int_{t_6^+}^{t_7^-} \left(\sum_{i=2}^6 |\tau_i| \right) dt \right\}. \quad (41)$$

The constraints are as follows:

$$\begin{aligned} q_i(t)|_{t=t_6^+} &= q_i(t_6^+), \\ \dot{q}_i(t)|_{t=t_6^+} &= \dot{q}_i(t_6^+), \\ \ddot{q}_i(t)|_{t=t_6^+} &= \ddot{q}_i(t_6^+), \\ {}^W \dot{x}_B(t_7^-) &= w_{Bx} {}^W \dot{x}_B(t_6^+), \\ {}^W \dot{y}_B(t_7^-) &= w_{By} {}^W \dot{y}_B(t_6^+), \\ {}^W x_G &= L, \\ {}^W y_G &= 0, \\ {}^W \dot{x}_G &= {}^W \dot{y}_G = {}^W \ddot{x}_G = {}^W \ddot{y}_G = 0, \\ {}^W x_A &= L - L_s, \\ {}^W y_A &= 0, \\ {}^W \dot{x}_A &= {}^W \dot{y}_A = {}^W \ddot{x}_A = {}^W \ddot{y}_A = 0, \\ {}^W x_{CM}(t) &= \frac{\sum_{i=1}^6 m_i {}^W x_{cmi}(t)}{\sum_{i=1}^6 m_i}, \\ {}^W y_{CM}(t) &= \frac{\sum_{i=1}^6 m_i {}^W y_{cmi}(t)}{\sum_{i=1}^6 m_i}, \\ {}^W \dot{x}_{CM}(t) &= \frac{\sum_{i=1}^6 m_i {}^W \dot{x}_{cmi}(t)}{\sum_{i=1}^6 m_i}, \\ {}^W \dot{y}_{CM}(t) &= \frac{\sum_{i=1}^6 m_i {}^W \dot{y}_{cmi}(t)}{\sum_{i=1}^6 m_i}, \\ {}^W \ddot{x}_{CM}(t) &= \frac{\sum_{i=1}^6 m_i {}^W \ddot{x}_{cmi}(t)}{\sum_{i=1}^6 m_i}, \\ {}^W \ddot{y}_{CM}(t) &= \frac{\sum_{i=1}^6 m_i {}^W \ddot{y}_{cmi}(t)}{\sum_{i=1}^6 m_i}, \\ X_{ZMP} &\in S_{\text{contact}}, \\ q_{\text{down}} &\leq q_i \leq q_{\text{iup}}, \\ \tau_{\text{down}} &\leq \tau_i \leq \tau_{\text{iup}}. \end{aligned} \quad (42)$$

(3) *Joint Trajectory Planning at the Landing III Subphase.* The rear leg and foreleg contact with the ground at the landing III subphase. The task of planning trajectory is to adjust

the posture of the robot for the next jump. Joint angular displacement, velocity, and acceleration are calculated using an identical method to what is presented in Joint Trajectory Planning at the Landing II Subphase. Given the consumed time, centroid position, and velocity at the end of the landing III subphase, the trajectories of active joints are depicted as follows:

$$q_i(t) = a_{i8}t^8 + a_{i7}t^7 + a_{i6}t^6 + a_{i5}t^5 + a_{i4}t^4 + a_{i3}t^3 + a_{i2}t^2 + a_{i1}t + a_{i0}, \quad t \in [t_7^+, t_8]. \quad (43)$$

a_i and b_i are parameters to be optimized. The object function is established to minimize the total consumed active torque as follows:

$$J = \min \left\{ \int_{t_7}^{t_8} \left(\sum_{i=2}^6 |\tau_i| \right) dt \right\}. \quad (44)$$

The constraints are as follows:

$$\begin{aligned} q_i(t)|_{t=t_7^+} &= q_i(t_7^+), \\ q_i(t)|_{t=t_8} &= q_i(t_8), \\ q_1 &= \pi, \\ {}^w x_G &= L, \\ {}^w y_G &= {}^w y_A = 0, \\ {}^w x_A &= L - L_s, \\ \dot{q}_i(t)|_{t=t_7^+} &= \dot{q}_i(t_7^+), \\ \ddot{q}_i(t)|_{t=t_7^+} &= \ddot{q}_i(t_7^+), \\ \dot{q}_i(t)|_{t=t_8} &= \ddot{q}_i(t)|_{t=t_8} = 0, \\ \dot{q}_1 &= \ddot{q}_1 = 0, \\ {}^w \dot{x}_G &= {}^w \dot{y}_G = {}^w \ddot{x}_G = {}^w \ddot{y}_G = 0, \\ {}^w \dot{x}_A &= {}^w \dot{y}_A = {}^w \ddot{x}_A = {}^w \ddot{y}_A = 0, \\ {}^w x_{CM}(t) &= \frac{\sum_{i=1}^6 m_i {}^w x_{cmi}(t)}{\sum_{i=1}^6 m_i}, \\ {}^w y_{CM}(t) &= \frac{\sum_{i=1}^6 m_i {}^w y_{cmi}(t)}{\sum_{i=1}^6 m_i}, \\ {}^w \dot{x}_{CM}(t) &= \frac{\sum_{i=1}^6 m_i {}^w \dot{x}_{cmi}(t)}{\sum_{i=1}^6 m_i}, \\ {}^w \dot{y}_{CM}(t) &= \frac{\sum_{i=1}^6 m_i {}^w \dot{y}_{cmi}(t)}{\sum_{i=1}^6 m_i}, \\ {}^w \ddot{x}_{CM}(t) &= \frac{\sum_{i=1}^6 m_i {}^w \ddot{x}_{cmi}(t)}{\sum_{i=1}^6 m_i}, \end{aligned}$$

$$\begin{aligned} {}^w \ddot{y}_{CM}(t) &= \frac{\sum_{i=1}^6 m_i {}^w \ddot{y}_{cmi}(t)}{\sum_{i=1}^6 m_i}, \\ X_{ZMP} &\in S_{\text{contact}}, \\ q_{i\text{down}} &\leq q_i \leq q_{i\text{up}}, \\ \tau_{i\text{down}} &\leq \tau_i \leq \tau_{i\text{up}}. \end{aligned} \quad (45)$$

4. Experiments and Discussions

The schematic diagram of the robot platform is shown in Figure 5. The computer is responsible for controlling the algorithm and human interaction. The air compressor supplies compressed air for the robot. The AD/DA card samples angular displacements of joints and pressure of pneumatic muscles and sends controlling commands to proportional valves. The amount of air inside pneumatic muscles is controlled by proportional valves. The Radial Basis Function Neural Network- (RBFNN-) tuned PID cascade controlling scheme (shown in Figure 6) is used to realize the closed-loop control of active joints. To speed up the calculation of the cascade PID controller, we adopted TMS320F28335 as the processor. This controller has a processing capacity of 150 MHz and is fast enough for the robot. More detailed information of the pressure sensor, potentiometer, and force sensor can be acquired from the Internet and are listed in Table 1.

The jumping experiment is performed using the planned active joint trajectories. In this paper, the desired maximum jumping height of the centroid trajectory is 360 mm and the desired jumping distance of the centroid trajectory is 730 mm. Given initial joint angles, the initial centroid position is (100, 160) [mm]. Given the centroid position at the start and end of the airborne phase, the time consumed at the initial phase is 180 ms, the time consumed at the initial jumping posture 150 ms, and other information, active joint trajectories are optimized in Figure 7. It is observed that angular variations of the knee joint and hip joint at the takeoff stage are larger than those of the ankle joint. The reason is that motions of the knee joint and hip joint produce pressure to the ankle joint. During the airborne phase, angular displacement of the ankle joint increases at first, then decreases gradually, while the angular displacement of the knee joint decreases at first, then increases. The above motion rotates the robot around its own centroid and prepares for landing of the foreleg. Angular displacement of the shoulder joint varies slowly at first, then rapidly changes, cooperating with the elbow joint, to reduce the speed of the hand of the robot and collision with the ground. No sudden change of angular displacements of active joints happens, while sharp changes of velocities of active joints occur, which indicates that collision between the robot and the ground happens.

The jumping process of the robot is shown in Figure 8. Firstly, the initial posture of the robot is adjusted according to the desired command. Secondly, the robot starts its jumping motion. At the end of the jumping II subphase, the foreleg of the robot leaves the ground, while

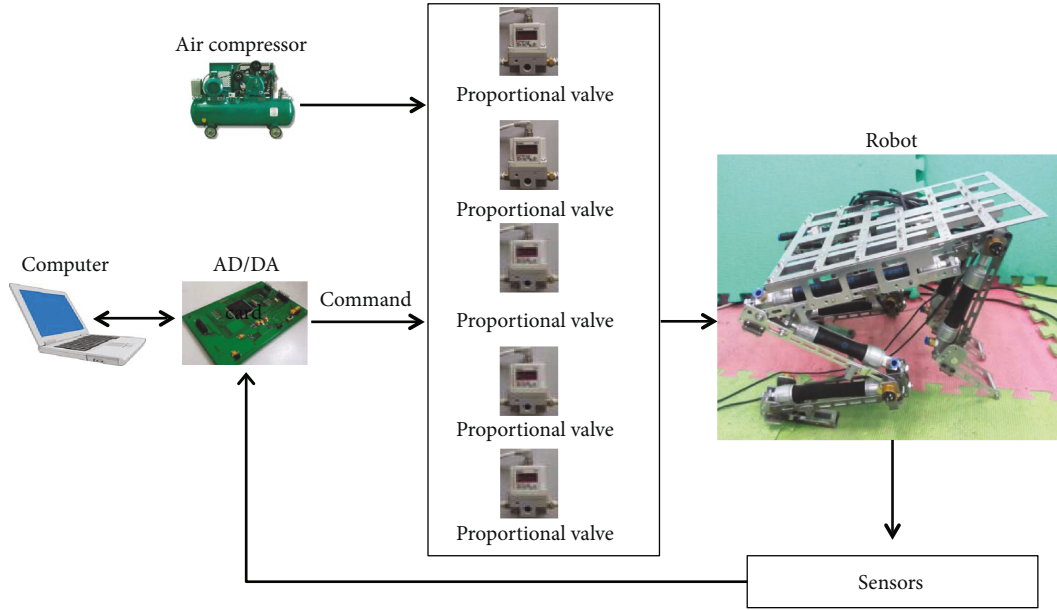


FIGURE 5: The schematic diagram of the robot platform.

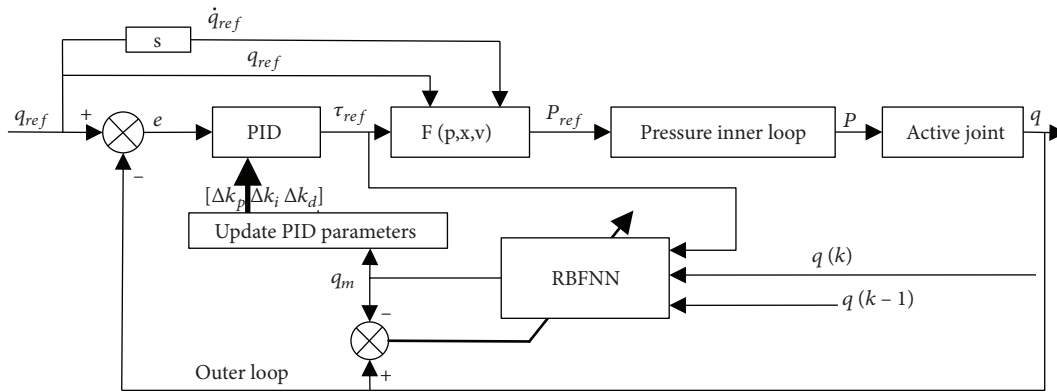


FIGURE 6: Control scheme of active joint of the robot.

TABLE 1: Sensors used in the robot.

Name	Measurement range	Output signal	Repeat accuracy	Working power
Pressure sensor PSE510	[0, 1] MPa	[0, 5] V	$\pm 0.3\%$ (F.S.)	DC 24 V
Potentiometer WDD22A 10K	[0, 360°]	[0, 5] V	$\pm 0.5\%$ (F.S.)	DC 5 V
Force sensor XH32	[-200, 200] kg	[-5, 5] V	$\pm 0.5\%$ (F.S.)	DC 5 V

the feet still coincide with the ground. An underactuated joint between the feet and the ground is created in the jumping III subphase. The posture of the robot is adjusted for landing by changing joint angles. During the landing II subphase, an underactuated joint is created between the feet and the ground, and velocity of the toe is decreased for stable landing. After entering the landing III subphase, active joints are regulated to the desired status for the next jumping motion.

The actual trajectories are listed in Figure 7. From comparison of desired trajectories and actual trajectories, maximum tracking errors of the ankle joint, knee joint, hip joint, shoulder joint, and elbow joint are 12.07°, 8.22°, 8.54°, 11.66°, and 2.65°, respectively, whilst standard deviation of tracking errors are 3.4°, 2.25°, 2.17°, 2.86°, and 0.77°, respectively. The inconsistency between the two rear legs in the jumping motion is due to mismachining tolerance, assembly errors, and tracheal disturbance.

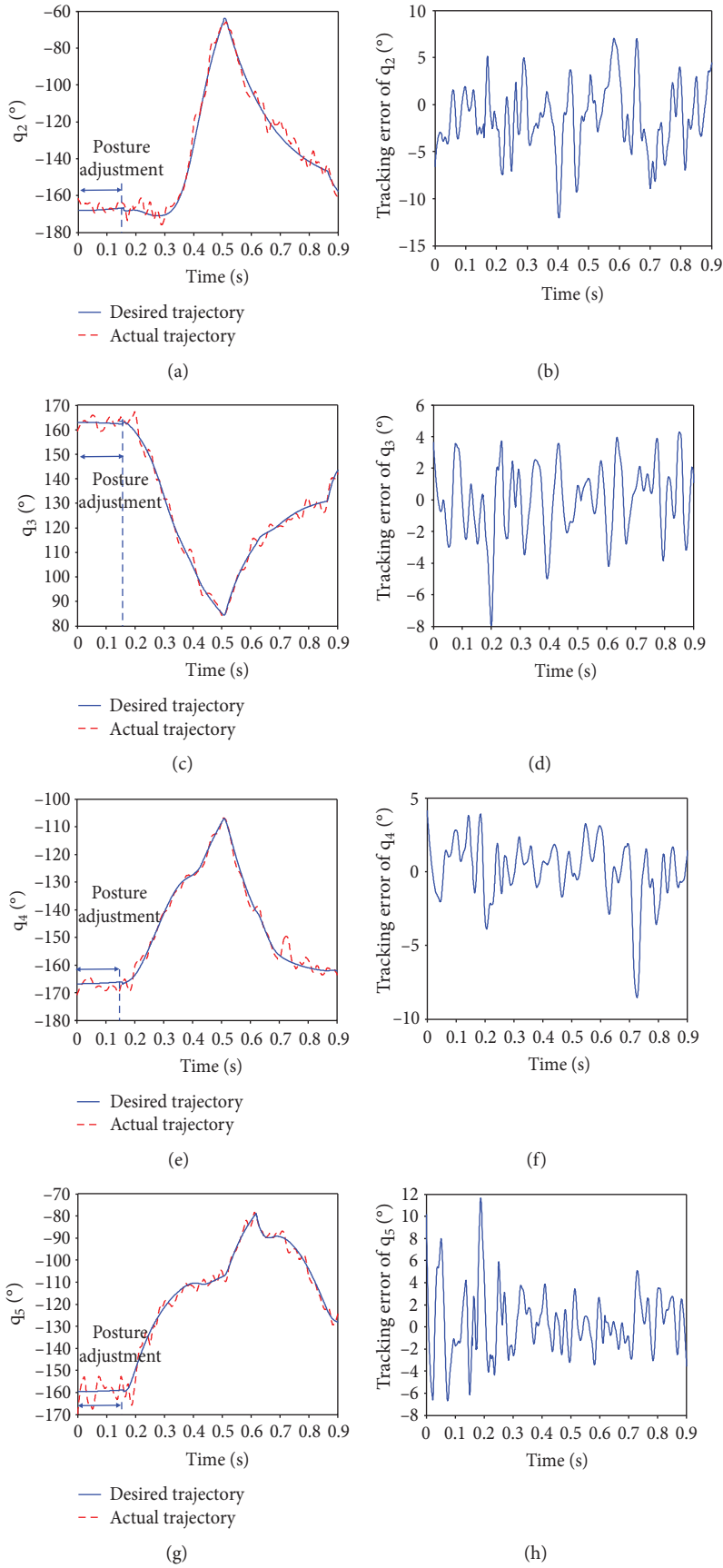


FIGURE 7: Continued.

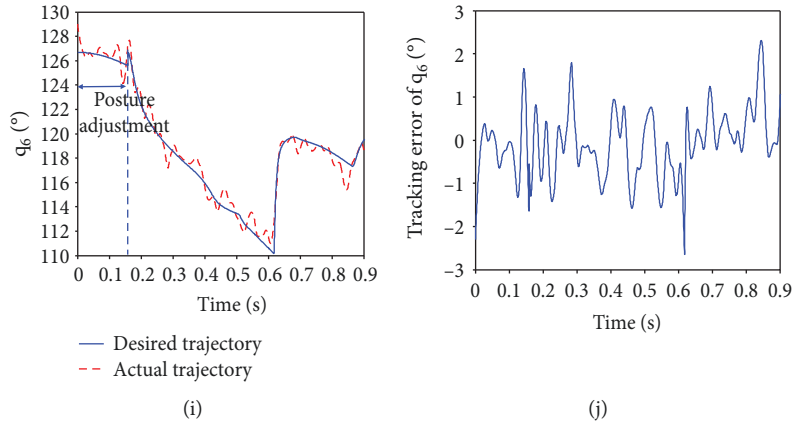


FIGURE 7: Trajectory tracking of active joints: (a), (c), (e), (g), and (i) are the trajectory tracking of the ankle joint, knee joint, hip joint, shoulder joint, and elbow joint, respectively; (b), (d), (f), (h), and (j) are the tracking errors of the ankle joint, knee joint, hip joint, shoulder joint, and elbow joint, respectively.

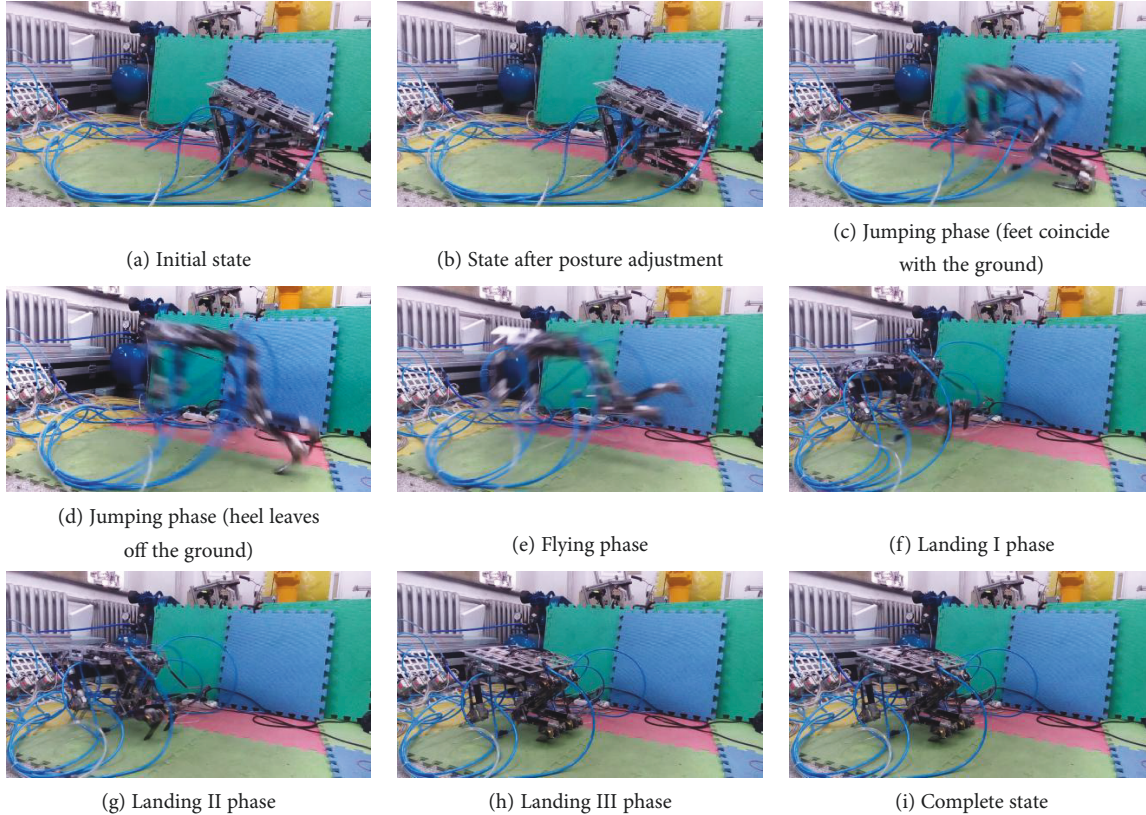


FIGURE 8: Robot jumping experiment.

5. Conclusion

This paper studies trajectory planning of an intermittent jumping quadruped robot driven by pneumatic muscle actuators and owning variable redundant and underactuated joints. The task of trajectory planning is performed in the centroid space and joint space. Trajectory planning in the centroid space is optimized by minimizing the

peak reaction force from the ground. Trajectory planning in the joint space is acquired by mapping the planned centroid trajectory. Initial posture of the robot is optimized by maximizing the specific direction vector along with the operable ellipsoid of generalized centroid velocity. Comparison between desired joint trajectory and actual performance indicates the validity of the trajectory planning method.

Data Availability

No additional data are available.

Conflicts of Interest

The authors declare that there is no conflict of interests regarding the publication of this paper.

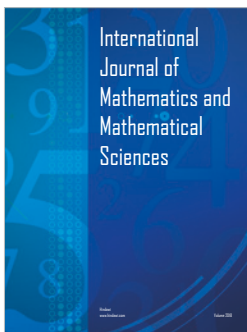
Acknowledgments

This work is supported by Natural Science Foundation of Jiangsu Province (BK20170301), the Fundamental Research Funds for the Central Universities (2016B11814), Jiangsu Province key development program (BE2017647), Science and technology planning projects of Changzhou (CJ20179042), Projects of International Cooperation and Exchanges of Changzhou (CZ20170018).

References

- [1] J. H. Park and S. Chung, "Optimal locomotion trajectory for biped robot 'D²' with knees stretched, heel-contact landings, and toe-off liftoffs," *Journal of Mechanical Science and Technology*, vol. 25, Supplement 1, pp. 3231–3241, 2011.
- [2] X. Wan, T. Urakubo, and Y. Tada, "Landing motion of a legged robot with impact force reduction and joint torque minimization," in *2013 Second International Conference on Robot, Vision and Signal Processing*, pp. 259–264, Kitakyushu, Japan, 2013.
- [3] B. Ugurlu and A. Kawamura, "Real-time running and jumping pattern generation for bipedal robots based on ZMP and Euler's equations," in *2009 IEEE/RSJ International Conference on Intelligent Robots and Systems*, pp. 1100–1105, St. Louis, MO, USA, 2009.
- [4] G. Bingwei, W. Sikai, and G. Yuanfeng, "Single leg vertical hopping gait planning for hydraulic quadruped robot," *Chinese Journal of Scientific Instrument*, vol. 5, 2017.
- [5] H. Xiao, H.-X. Sun, Y.-H. Zhang, and Q.-X. Jia, "Dynamics modeling and obstacle-navigation control of a two-wheel robot with jumping ability," *Development & Innovation of Machinery & Electrical Products*, vol. 26, no. 6, pp. 4–7, 2013.
- [6] S. W. Kim, J. S. Koh, J. G. Lee, J. Ryu, M. Cho, and K. J. Cho, "Flytrap-inspired robot using structurally integrated actuation based on bistability and a developable surface," *Bioinspiration & Biomimetics*, vol. 9, no. 3, 2014.
- [7] H. U. Sheng-Hai, D. E. Kun-xiu, G. U. Bin, and X. U. Peng, "Take-off task planning and control for bionic frog jumping robot," *Computer Simulation*, vol. 30, no. 7, pp. 341–344, 2013.
- [8] K. Deng, B. Guo, P. Xu, and L. Li, "Analysis of motion planning and take-off mechanism for a multi-joint jumping robot," *Applied Science and Technology*, vol. 39, no. 4, pp. 25–30, 2012.
- [9] F. Jing, Y. Qi, Y. Qiang, and C. Yang, "An on-line robot trajectory planning algorithm in joint space with continuous accelerations," in *International Conference on Advanced Technology of Design and Manufacture (ATDM 2010)*, pp. 372–377, Beijing, China, 2010.
- [10] J. Yuan, H. Chen, F. Sun, and Y. Huang, "Trajectory planning and tracking control for autonomous bicycle robot," *Nonlinear Dynamics*, vol. 78, no. 1, pp. 421–431, 2014.
- [11] X. Wan, T. Urakubo, and Y. Tada, "Optimization of jumping motion of a legged robot for different take-off postures," *Journal of Mechanical Science and Technology*, vol. 29, no. 4, pp. 1391–1397, 2015.
- [12] Z. Xu, T. Lü, and F. Ling, "Trajectory planning of jumping over obstacles for hopping robot," *Journal of the Brazilian Society of Mechanical Sciences and Engineering*, vol. 30, no. 4, pp. 327–334, 2008.
- [13] K. V. Heerden and A. Kawamura, "Towards integrated walking and jumping motion planning in complex environments: jumping trajectory generation," in *2012 12th IEEE International Workshop on Advanced Motion Control (AMC)*, pp. 1–6, Sarajevo, Bosnia-Herzegovina, 2012.
- [14] A. Kawamura and K. V. Heerden, "Maintaining floor-foot contact of a biped robot by force constraint position control," in *2011 IEEE International Conference on Mechatronics*, pp. 857–862, Istanbul, Turkey, 2011.
- [15] D. Aversa, S. Sardina, and S. Vassos, "Path planning with inventory-driven Jump-Point-Search," in *Proceedings of the AAAI Conference on Artificial Intelligence and Interactive Digital Entertainment (AIIDE)*, pp. 14–18, Santa Cruz, CA, USA, 2015.
- [16] D. Lakatos, D. Seidel, W. Friedl, and A. Albu-Schaffer, "Targeted jumping of compliantly actuated hoppers based on discrete planning and switching control," in *2015 IEEE/RSJ International Conference on Intelligent Robots and Systems (IROS)*, pp. 5802–5808, Hamburg, Germany, 2015.
- [17] C. Yang, K. Huang, H. Cheng, Y. Li, and C. Y. Su, "Haptic identification by ELM-controlled uncertain manipulator," *IEEE Transactions on Systems, Man, and Cybernetics: Systems*, vol. 47, no. 8, pp. 2398–2409, 2017.
- [18] D. Constantinescu and E. A. Croft, "Smooth and time-optimal trajectory planning for industrial manipulators along specified paths," *Journal of Robotic Systems*, vol. 17, no. 5, pp. 233–249, 2000.
- [19] H. Liu, X. Lai, and W. Wu, "Time-optimal and jerk-continuous trajectory planning for robot manipulators with kinematic constraints," *Robotics and Computer-Integrated Manufacturing*, vol. 29, no. 2, pp. 309–317, 2013.
- [20] L. M. Capisani and A. Ferrara, "Trajectory planning and second-order sliding mode motion/interaction control for robot manipulators in unknown environments," *IEEE Transactions on Industrial Electronics*, vol. 59, no. 8, pp. 3189–3198, 2012.
- [21] R. Qi, W. Zhou, and T. Wang, "An obstacle avoidance trajectory planning scheme for space manipulators based on genetic algorithm," *Robot*, vol. 36, no. 3, pp. 263–270, 2014.
- [22] C. Wang, X. Liu, X. Yang, F. Hu, A. Jiang, and C. Yang, "Trajectory tracking of an omni-directional wheeled mobile robot using a model predictive control strategy," *Applied Sciences*, vol. 8, no. 2, p. 231, 2018.
- [23] T. Lolla, P. F. J. Lermusiaux, M. P. Ueckermann, and P. J. Haley, "Time-optimal path planning in dynamic flows using level set equations: theory and schemes," *Ocean Dynamics*, vol. 64, no. 10, pp. 1373–1397, 2014.
- [24] J. Zhong, *Research on Frog-Inspired Biomimetic Jumping Robot Actuated by Pneumatic Muscles and its Key Technologies*, Harbin Institute of Technology, 2015.

- [25] B. Ugurlu and A. Kawamura, "ZMP-based online jumping pattern generation for a one-legged robot," *IEEE Transactions on Industrial Electronics*, vol. 57, no. 5, pp. 1701–1709, 2010.
- [26] P. W. Chen, G. E. Wen-Jie, and H. J. Dong, "Research on landing stability of hopping robot considering flexible joint," *Journal of Machine Design*, vol. 30, no. 1, pp. 35–39, 2013.




Hindawi

Submit your manuscripts at
www.hindawi.com

